PHYSICAL REVIEW VOLUME 169, NUMBER 5 25 MAY 1968

$SU(6)$ Invariance in s-Wave Meson-Baryon Scattering

DAVID C. CAREY*
University of Michigan, Ann Arbor, Michigan
(Received 17 November 1967)

$SU(6)$ has been incorporated into a simple model of a multichannel amplitude for s-wave scattering of mesons in the **35** representation by baryons in the **56**. Symmetry breaking is introduced by making the amplitude satisfy unitarity exactly in the direct channel. The contributions to the amplitude from the crossed-channel singularities are assumed to be $SU(6)$-invariant, and can be expressed in terms of four scattering lengths by the use of appropriate projection matrices. Fits of the model have been made to the threshold parameters of πN, KN, and $\bar{K}N$ scattering. Several solutions have been found, and a comparison of calculated threshold parameters, cross sections, and phase shifts with experimental data is made. Calculations of resonances predicted by the model are performed and found to be in good agreement with experimental results.

I. INTRODUCTION

RECENT meson-baryon scattering experiments and pion-nucleon phase-shift analyses have revealed an s-wave resonant structure heretofore unsuspected. Several papers have been published which attempt to analyze the available data and reproduce this resonant structure. Those models which incorporate $SU(3)$ have the advantage that they permit an $SU(3)$ classification of s-wave resonant states. Wyld[1] has performed a calculation with a coupled-channel Schrödinger equation incorporating $SU(3)$ in a static-model vector-meson-exchange potential, and is able to reproduce many of the low-energy s-wave resonances. Brehm[2] has attacked the same problem for the πN system in a dispersion-theory framework and has calculated one S_{11} resonance. The present paper is an adaptation of an idea due to Ross,[3] namely, that of including higher symmetries in an effective-range approximation. Ross considered the problem where $SU(3)$ is the higher symmetry involved. Since the Kronecker product of two $SU(3)$ octets yields a singlet, two octets, a decuplet, a conjugate decuplet, and a **27**, we have six scattering lengths and a mixing parameter between the octets for fitting. Here we employ $SU(6)$ in a modification of the usual effective-range approximation. Since Gyuk and Tuan[4] have recently made an analysis of s-wave resonances and place the low-lying ones in the **70** representation of $SU(6)$, it seems appropriate to calculate the s-wave resonant structure in terms of $SU(6)$. Application of a model involving $SU(6)$ to higher partial waves would be much riskier since $SU(6)$ symmetry involves the assumption of spin invariance[5] and only in the s wave with $l=0$ are effects of spin-orbit coupling completely absent.

In $SU(6)$ theory, the pseudoscalar and vector mesons are commonly placed in the **35** representation. The baryons and baryon resonances are placed in the **56**.[6] Since the decomposition of the product of these two into irreducible representations yields **56+70+700+1134**, we have only four parameters to vary in fitting the data. Furthermore, by using $SU(6)$, we may consider the effect of inelastic channels with higher thresholds. The cross sections for resonance production have not been explicitly calculated with our model, since they invariably involve many more partial waves than just the s wave. However, the inclusion of resonance states provides a first approximation to the inelasticity effects of multibody production through quasi-two-body channels, i.e., where the final products may be described in terms of two bodies, one or more of which is a resonance.

II. FORM OF THE AMPLITUDE

We write the S matrix as follows:

$$S_{fi}=\delta_{fi}-(2\pi)^4 i\delta^4(P_f-P_i)\frac{4\pi F_{fi}}{(4E_fE_i\omega_f\omega_i)^{1/2}},\qquad (1)$$

where P_i and P_f are initial and final total momenta, respectively, and E_i, ω_i and E_f, ω_f are initial and final baryon and meson energies, respectively. If we apply unitarity

$$SS^\dagger=I,\qquad (2)$$

sum over intermediate states, and take the s-wave component (we omit any subscript indicating the partial wave since we are dealing only with the s wave), we arrive at

$$F_{fi}-F_{fi}^\dagger=(2ik/W)F_{fn}F_{ni}^\dagger.\qquad (3)$$

We now make use of time-reversal invariance and choose our phases such that $F_{fi}^\dagger=F_{fi}^*$, arriving at

$$\mathrm{Im}F^{-1}=-k/W\qquad (4)$$

for any open channel with W being the total center-of-mass energy, and k a diagonal matrix giving the momentum in each channel in the center-of-mass

* Present address: City College of New York, New York, N. Y.
[1] H. W. Wyld, Jr., Phys. Rev. **155**, 1649 (1967).
[2] J. J. Brehm (unpublished).
[3] M. H. Ross, in *Proceedings of the Twelfth Annual Conference on High-Energy Physics, Dubna, 1964* (Atomizdat, Moscow, 1965).
[4] Imre P. Gyuk and S. F. Tuan, Phys. Rev. **140**, 164 (1965).
[5] H. J. Lipkin and S. Meshkov, Phys. Rev. **143**, 1269 (1966).
[6] F. Gürsey and L. A. Radicati, Phys. Rev. Letters **13**, 173 (1964).

system. The center-of-mass momentum is computed as

$$k^2=[(W+M)^2-\mu^2][(W-M)^2-\mu^2]/4W^2, \quad (5)$$

where M and μ are the baryon and meson masses, respectively, in the given channel.

In order to make our function analytic save for the cuts due to unitarity, we define a function g as follows:

$$g(\nu)=-\frac{\nu}{\pi}\int\frac{k'}{W'}\frac{1}{\nu'}\frac{d\nu'}{\nu'-\nu}, \quad (6)$$

where $\nu=[W^2-(M+\mu)^2]/4M\mu$. It may be verified that $\mathrm{Im}g(\nu)=-k/W$ above threshold. One subtraction is made for convergence and the subtraction point is chosen so that $g(\nu)$ is zero at threshold. The center-of-mass momentum k expressed in terms of ν is

$$k=[\nu(\nu+1)]^{1/2}\times 2M\mu/W. \quad (7)$$

If we perform the integration we find that

$$g(\nu)=I_1+I_2, \quad (8)$$

where

$$I_1=B/W^2-B/(M+\mu)^2 \quad (9)$$

and

$$B=(1/\pi)(M^2-\mu^2)\ln[(M/\mu)^{1/2}]. \quad (10)$$

For $\nu>0$,

$$I_2=\frac{k}{W}\left[\frac{2}{\pi}\ln[\nu^{1/2}+(\nu+1)^{1/2}]-i\right]; \quad (11)$$

for $0>\nu>-1$,

$$I_2=\frac{\kappa}{W}\left\{1-\frac{2}{\pi}\tan^{-1}\left[\left(\frac{-\nu}{\nu+1}\right)^{1/2}\right]\right\};$$

for $-1>\nu$,

$$I_2=\frac{\kappa}{W}\left[\frac{2}{\pi}\ln[(-\nu)^{1/2}-(-\nu-1)^{1/2}]\right],$$

where, for $\nu<0$, κ^2 is computed as the absolute value of the expression for k^2. Since the k matrix is computed using the experimental masses, we are introducing symmetry breaking by making the amplitude satisfy unitarity. By using the function g, the nature of our assumptions becomes much clearer. The $SU(6)$ symmetry is broken only by the requirements of unitarity. Therefore, such symmetry-breaking effects are confined entirely to the contribution to the amplitude from the right-hand cut. The remainder of the amplitude, that due to the left-hand cuts, is then assumed to be $SU(6)$-symmetric. Such a separation of the contributions to the amplitude into those due to direct- and cross-channel cuts also makes our scattering-length approximation, described below, seem more reasonable. Since the cuts due to the cross channel will be more distant from the region of interest than those from the direct channel, it is reasonable to assume that they would be slowly varying with energy. Hence one is justified in replacing them by constants in the low-energy region.

The portion of the inverse amplitude due to cross-channel cuts is real, and all terms which contribute to it are assumed to be $SU(6)$-invariant. This means that it can be written as a sum of terms, each of which is the product of a projection matrix times the reciprocal of an $SU(6)$-invariant scattering length. Since the product of the **35** and **56** representations decomposes into four irreducible representations, we have four projection matrices and four scattering lengths. Each of the projection matrices projects the states in the product **35**$\times$**56** onto one of the four irreducible representations, **56**, **70**, **700**, or **1134**. We then have

$$\mathrm{Re}(F^{-1})=\sum_i\frac{1}{A_i}P_i+\mathrm{Re}g. \quad (12)$$

The projection matrices are computed by making a similarity transformation on a matrix which has ones and zeros on the diagonal and zeros elsewhere, via a matrix of Clebsch-Gordan coefficients, so that

$$P_i=CP_i'C, \quad (13)$$

with

$$P_i'=\begin{bmatrix}0 & & & & & & & & \\ & \cdot & & & & & & & \\ & & \cdot & & & & & & \\ & & & 1 & & & & & \\ & & & & \cdot & & & & \\ & & & & & 1 & & & \\ & & & & & & \cdot & & \\ & & & & & & & \cdot & \\ & & & & & & & & 0\end{bmatrix}. \quad (14)$$

A table of the projection matrices used is to be found in the Appendix to this paper. The Clebsch-Gordan coefficients were computed by using the tables of Carter, Coyne, and Meshkov[7] in conjunction with the isoscalar coefficients of de Swart.[8]

We have then as a final form

$$F_{fi}=\left[\sum_i\frac{1}{A_i}P_i+g\right]^{-1}. \quad (15)$$

The scattering lengths are taken as constants in the energy range under consideration. In our case we have chosen our normalization so that g is replaced by $W_0 g$, where W_0 is the center-of-mass energy at the pion-proton threshold. Thus in the pion-nucleon system at

[7] J. C. Carter, J. J. Coyne, and S. Meshkov, Phys. Rev. Letters 14, 523 (1965); 14, 850(E) (1965).

[8] J. J. de Swart, Rev. Mod. Phys. 35, 916 (1963).

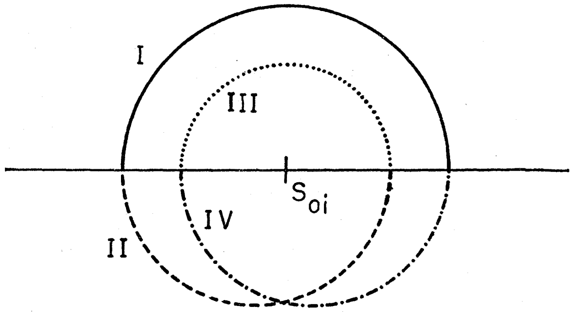

FIG. 1. Sheet structure in the vicinity of a given threshold.

threshold, our amplitude coincides with the more familiar form $f=(1/k)e^{i\delta}\sin\delta$, and our scattering lengths can be measured in fermis. Using our form for the amplitude, the cross section for a given process is given by

$$\sigma_{fi}=4\pi\frac{k_f}{k_i}\frac{1}{W^2}|F_{fi}|^2, \tag{16}$$

where k_i and k_f are the initial and final center-of-mass momenta, respectively.

III. LOW-ENERGY PARAMETERS

Because of the length of time it takes to invert a complex matrix on a computer, it was deemed impractical to attempt to fit to phase-shift or cross-section data. Instead we have chosen to fit to the small number of parameters which describe the threshold behavior of pseudoscalar-meson–baryon scattering.

In the kaon-nucleon and pion-nucleon systems, only the elastic channel is open in the neighborhood of threshold. Hence we can represent the low-energy data in terms of a single-channel effective-range formula

$$f=(W_0/W)F=(e^{i\delta}\sin\delta)/k\approx[(1/a)-ik]^{-1}, \tag{17}$$

where a is the conventional scattering length in the given channel and is given as the limit of $k\cot\delta$ as k approaches zero. At threshold, the amplitude f is equal to the scattering length, and thus can be given as above in terms of the elastic component of the F matrix evaluated at threshold. The two pion-nucleon scattering lengths are taken from the work of Hamilton,[9] and those for the kaon-nucleon system from Stenger *et al.*[10]

In the case of $\bar{K}$-nucleon scattering, the $\pi\Sigma$ and $\pi\Lambda$ channels are also open at threshold. Thus we cannot use a single-channel formula to represent the data. Dalitz and Tuan[11] have formulated a multichannel expression for the scattering amplitude. The elastic amplitude may still be written as an effective-range approximation

$$f=(e^{i\delta}\sin\delta)/k=[(1/A)-ik]^{-1}, \tag{18}$$

but because of the presence of inelastic channels, A will be complex, i.e., $A=a+ib$, giving a real and an imaginary part for the scattering length for both possible values of isotopic spin. There are two additional parameters which describe the inelastic channels. They are γ, the ratio of Σ^- to Σ^+ production at rest, and ϵ, the ratio of Λ production to total $I=1$ hyperon-pion production at rest, both in the K^-p system. In terms of the F matrix, we have

$$\gamma=\frac{k_{\Sigma^-\pi^+}|-\frac{1}{2}F_1^{\Sigma}-(1/\sqrt{6})F_0^{\Sigma}|^2}{k_{\Sigma^+\pi^-}|\frac{1}{2}F_1^{\Sigma}-(1/\sqrt{6})F_0^{\Sigma}|^2}, \tag{19}$$

where F_0 and F_1 are the $I=0$ and $I=1$ $\Sigma\pi$ production elements of the F matrix, respectively, and

$$\epsilon=\frac{k_{\Lambda\pi^0}|F_1|^2}{k_{\Lambda\pi}|F_1|^2+k_{\Sigma\pi}|F_1|^2}, \tag{20}$$

where again F_1 is the $\Lambda\pi$ production element of the $I=1$ F matrix. The values of the six Dalitz-Tuan parameters are taken from Sakitt *et al.*[12] They have two solutions, but we have used the numbers from the second only, since solution 1 is not consistent with the charge-exchange data of Kittel *et al.*[13] Also, only solution 2 gives agreement with an analysis of the K^-p scattering data at higher energies by Watson *et al.*[14]

A search in the four-dimensional space of the $SU(6)$-invariant scattering lengths A_i has been made, and an iteration from the points of lowest χ^2 was performed in order to obtain the best fits to the data. The errors used

TABLE I. Scattering lengths and low-energy parameters.

Parameter	Given (F)	Error (F)	Solution I (F)	Solution II (F)
A_{56}	...	...	0.939	−0.794
A_{70}	...	...	−0.842	0.396
A_{700}	...	...	−0.306	−0.345
A_{1134}	...	...	−0.168	0.694
		πN		
a_3	−0.129	0.1	−0.151	−0.151
a_1	0.246	0.1	0.172	0.234
		KN		
a_1	−0.31	0.1	−0.18	−0.09
a_0	0.04	0.1	−0.16	0.11
		$\bar{K}N$		
ReA_1	−0.19	0.15	0.00	−0.16
ImA_1	0.44	0.15	0.02	0.18
ReA_0	−1.63	0.15	−1.73	−1.59
ImA_0	0.51	0.15	0.53	0.04
γ	2.11	0.30	1.17	2.37
ϵ	0.31	0.10	0.29	0.06
χ^2	...	...	25.7	24.9

[9] J. Hamilton, Phys. Letters 20, 687 (1966).
[10] V. J. Stenger, W. E. Slater, D. H. Stork, H. K. Ticho, G. Goldhaber, and S. Goldhaber, Phys. Rev. 134, B1111 (1964).
[11] R. H. Dalitz and S. F. Tuan, Ann. Phys. (N. Y.) 10, 307 (1960).
[12] M. Sakitt, T. B. Day, R. G. Glasser, N. Seeman, J. Friedman, W. E. Humphrey, and R. R. Ross, Phys. Rev. 139, B719 (1965).
[13] W. Kittel, G. Otter, and I. Wacek, Phys. Letters 21, 349 (1966).
[14] Mason B. Watson, Massimiliano Ferro-Luzzi, and Robert D. Tripp, Phys. Rev. 131, 2248 (1963).

TABLE II. Spin-$\frac{1}{2}$ s-wave baryon resonances in the **70**.

Name	Spin and parity	Isotopic spin	Mass (MeV)	Width (MeV)
		$SU(3)$ singlet		
Y_0^*	$\frac{1}{2}^-$	0	1405	35
		$SU(3)$ octet		
$\tilde{N}$	$\frac{1}{2}^-$	$\frac{1}{2}$	1570	130
$\tilde{\Sigma}$	...	...	...	...
$\tilde{\Lambda}$	$\frac{1}{2}^-$	0	1670	18
$\tilde{\Xi}$	...	...	...	...
		$SU(3)$ decuplet		
$\tilde{N}^*$	$\frac{1}{2}^-$	$\frac{3}{2}$	1670	180
$\tilde{Y}_1^*$	...	...	...	...
$\tilde{\Xi}^*$	...	...	...	...
Ω	...	...	...	...

in computing the χ^2 have nothing to do with actual experimental errors, but merely serve as weights for the given parameters in order to obtain what seemed subjectively to be the best fit. For example, the errors for the parameters of the $\bar{K}N$ channel are larger since there are more parameters to fit. However, it was observed that the final solution is quite insensitive to the relative errors used. The value of χ^2 is therefore of little significance except as a comparison of different sets of parameters.

Two solutions were found which were significantly better than any others observed. Since the values of the calculated low-energy parameters are rather sensitive to changes in the four scattering lengths, any exhaustive search must involve an extremely fine mesh. Hence it is possible that there exist other solutions as good as the ones located. The four scattering lengths and low-energy parameters for each solution along with the accepted values are given in Table I.

IV. COMPARISON WITH EXPERIMENT

A. General Remarks

To compare our model further with experimental results, we can calculate phase shifts and cross sections and also look for poles of the amplitude and attempt to identify them with known resonances.

Since the function giving the center-of-mass momentum k of two particles in terms of the total energy W of the system involves a square root, our amplitude has a branch point at each two-particle threshold and is a multisheeted function of the complex variable $s=W^2$. The number of sheets is equal to 2 to a power equal to the number of two-body channels in the amplitude. The sheet structure in the vicinity of a given threshold s_{0i} of channel i is illustrated in Fig. 1. The cut to the left of s_{0i} is due to all channels with lower thresholds than s_{0i}. The cut to the right of s_{0i} has a contribution from channel i also. The labeling of the sheets in the picture is relevant only in the vicinity of s_{0i}. However, it can be used to indicate a given sheet of the scattering amplitude in terms of the path needed to reach it from the physical sheet.

A resonance in a given two-body system is associated with a pole in the scattering amplitude. We have searched for resonances by searching for zeros of the real part of the determinant D of the inverse amplitude on the real axis. Since any pole in the scattering amplitude near the physical sheet (sheet I) may cause resonant behavior, it is clear that we must investigate the possibility of a pole on all such sheets. For instance, a pole on sheet IV slightly below s_{0i} will cause resonant behavior in the production of particles in channel i. Since, in our model, the thresholds are all well separated, it is clear that we need consider only those sheets which may be reached in the manner indicated in Fig. 1, i.e., by moving around a single branch point. Our search for poles was made by finding the zeros of ReD on the real axis as approached from sheet I or the analog of sheet III with respect to a given threshold. Since this still involves a large number of sheets, we have considered only cases connected with established resonances.

Gyuk and Tuan[4] have argued that a number of s-wave baryon resonances are to be placed in the **70** representation of $SU(6)$. Broken down according to $SU(3)\times SU(2)$, the **70** representation contains a spin-$\frac{1}{2}$ $SU(3)$ singlet, a spin-$\frac{3}{2}$ octet, a spin-$\frac{1}{2}$ octet, and a spin-$\frac{1}{2}$ decuplet. They identify the singlet with the $Y_0^*(1405)$. The spin-$\frac{3}{2}$ octet does not enter into our considerations since our amplitude is for total angular momentum $\frac{1}{2}$. The spin-$\frac{1}{2}$ octet contains the resonances seen in η production. In addition to the $\tilde{N}(1570)$ and the $\tilde{\Lambda}(1670)$, there should be a $\tilde{\Sigma}$ and a $\tilde{\Xi}$. The $\tilde{\Sigma}$ might be found in our $Y=0$, $I=1$ amplitude. Only the $\tilde{N}^*(1670)$ member of the decuplet has been observed experimentally. In addition there should be a $\tilde{Y}_1^*$, a $\tilde{\Xi}^*$, and an $\tilde{\Omega}$. Of these only the $\tilde{Y}_1^*$ might be reflected in our amplitude. A list of established s-wave, spin-$\frac{1}{2}$ resonances and those predicted by $SU(6)$ is presented in Table II. Those predicted by our results are listed in Table III. The expression used to evaluate the width of a resonance is given by $2\,\mathrm{Im}D/(d\,\mathrm{Re}D/dW)$, evaluated at the zero

TABLE III. Predicted resonances.

Name	Sheet	I	Y	Mass (MeV)	Width (MeV)
		Solution I			
$N_{3/2}^*$	...	$\frac{3}{2}$	1	1594	217
$N_{1/2}^*$	...	$\frac{1}{2}$	1	1417	258
Y_1^*	...	1	0	1563	105
Y_0^*	...	0	0	1375	138
Y_0^*	$\eta\Lambda$	0	0	1670	330
		Solution II			
$N_{3/2}^*$	...	$\frac{3}{2}$	1	2100	
$N_{1/2}^*$	...	$\frac{1}{2}$	1	1355	144
Y_1^*	...	1	0	1327	0.1
Y_0^*	...	0	0	1415	2

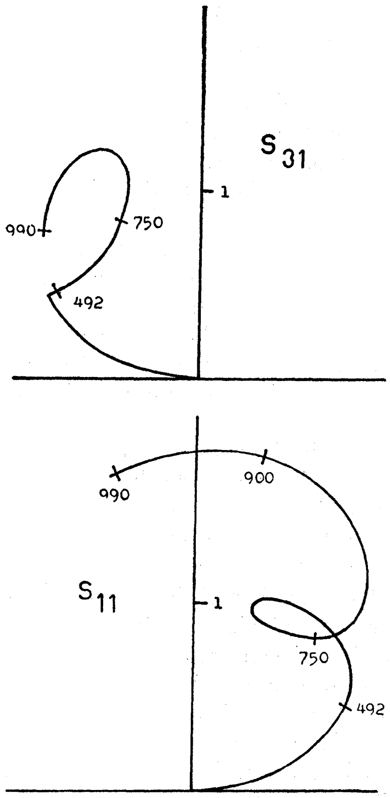

FIG. 2. Argand diagram of s-wave amplitude for pion-nucleon scattering. Function plotted is $2kf=(e^{2i\delta}-1)/i$. Notation is $S_{2I,2J}$. Data is by Bareyre *et al.* (Ref. 15).

of ReD. This expression holds good if ImD is a slowly varying function of W compared to ReD, as seems usually to be the case. Recurrences of given resonances on more than one sheet are not listed, and the sheet is given only if the resonance is seen only from somewhere other than the real axis as approached from sheet I. In this latter case, the zero of ReD is on the real axis as approached from sheet III with respect to the threshold indicated.

B. Pion-Nucleon System, $Y=1$

Only for pion-nucleon elastic scattering does there exist a well-defined set of phase shifts. For all other channels we must compare directly with cross-section data. However, many of the channels exhibit strong contributions from higher partial waves. If we are to compare an experimental cross section with a theoretical value calculated from an s-wave amplitude, we must restrict ourselves to processes which are dominated by s waves. In the case of pion-nucleon elastic scattering we can compare directly with existing sets of phase shifts. For comparison, in the $I=\frac{3}{2}$ channel we have plotted the results of Bareyre *et al.*,[15] Donnachie *et al.*,[16] and Bransden *et al.*[17] in Figs. 2–4. The graph is an Argand diagram of the function $2kf=(\eta e^{2i\delta}-1)/i$ and the incident pion kinetic energy in MeV is indicated at points along the curve. When the elasticity $\eta=1$, the curve falls on the circumference of a circle with radius 1 and center at i. For $\eta<1$, the graph falls inside this circle. Qualitatively, the analyses of Bareyre *et al.* and Donnachie *et al.* are very similar, while that of Bransden *et al.* seems rather peculiar. In fact, it is difficult to see how the phase shift is to be a continuous function of energy in this latter case. In the two former cases, a resonance of about 1670 MeV is definitely indicated. Such a resonance, having $I=\frac{3}{2}$, would probably belong to the **10** representation of $SU(3)$. For the $I=\frac{1}{2}$ channel, we have plotted the results of Bareyre *et al.*, Lovelace *et al.*,[18] and Bransden *et al.*, also in Figs. 2–4. In all three cases, a resonance can be seen at about 1570 MeV. However, the quantitative aspects of the resonance vary significantly among the three plots. In the first and third cases, an additional resonance is observed at 1700 MeV. The problem of assignment to a representation of $SU(6)$ will be considered only for the first of these two resonances.

A comparison of the pion-nucleon phase shifts predicted by our model with the values derived in various phase-shift analyses is quite impressive in some respects

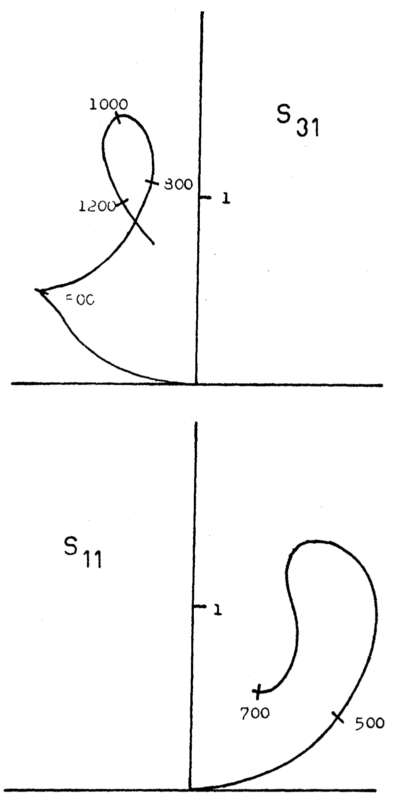

FIG. 3. Same graph as Fig. 2. Data for S_{31} by Donnachie *et al.* (Ref. 16). Data for S_{11} by Lovelace *et al.* (Ref. 18).

[15] P. Bareyre, C. Brickman, A. V. Stirling, and G. Villet, Phys. Letters **18**, 342 (1965).

[16] A. Donnachie, A. T. Lea, and C. Lovelace, Phys. Letters **19**, 146 (1965).

[17] B. H. Bransden, P. J. O'Donnell, and R. G. Moorhouse, Phys. Rev. **139**, B1566 (1965); Phys. Letters **19**, 420 (1965).

[18] C. Lovelace, Proc. Roy. Soc. (London) **A289**, 547 (1966).

and less so in others. Curves may be seen in Figs. 5 and 6 for solutions I and II, respectively. In all cases, the elasticity η predicted by our model is much too great. A possible explanation for such a high value of η may be the fact that only two-body s-wave channels were considered. In such a model the lowest inelastic threshold is $K\Sigma$ at 1683-MeV center-of-mass energy in the $I=\frac{3}{2}$ channel, and ηn at 1488 MeV in the $I=\frac{1}{2}$ channel. However, if we consider the possibility of other than s waves, the production of d wave $\pi N^*(1236)$ can occur in both isotopic spins and has a threshold of 1376 MeV. Other channels with numbers of particles greater than two, such as nonresonant $\pi N \rightarrow \pi\pi N$, might further contribute to the elasticity. In the $I=\frac{3}{2}$ channel, the elasticity η starts differing significantly from 1 at an incident pion kinetic energy of about 500 MeV, or a total center-of-mass energy of 1450 MeV, so the contribution of higher partial waves is significant. However, in the $I=\frac{1}{2}$ system, inelasticity begins at a pion kinetic energy of about 600 MeV, or the vicinity of the ηn threshold. Also, as shown by Richards,[19] the process $\pi^- p \rightarrow \eta n$ does account for the major portion of the inelasticity in the $I=\frac{1}{2}$ channel. This particular reaction is discussed in more detail below.

In the $I=\frac{3}{2}$ channel, the S_{31} resonance at about 1700 MeV is highly inelastic and the phase shift always

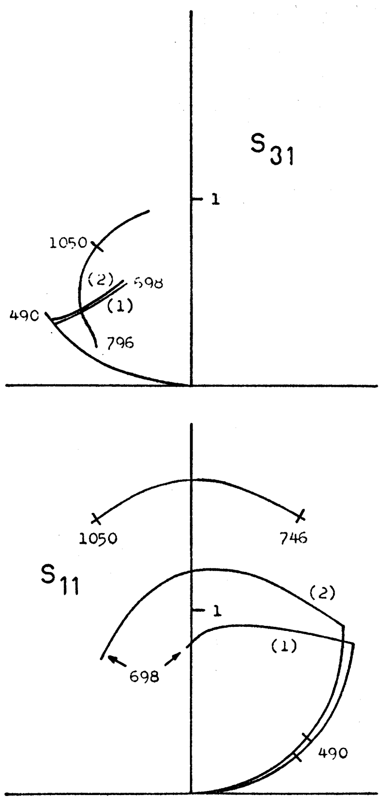

FIG. 4. Same graph as Fig. 2. Data by Bransden *et al.* (Ref. 17).

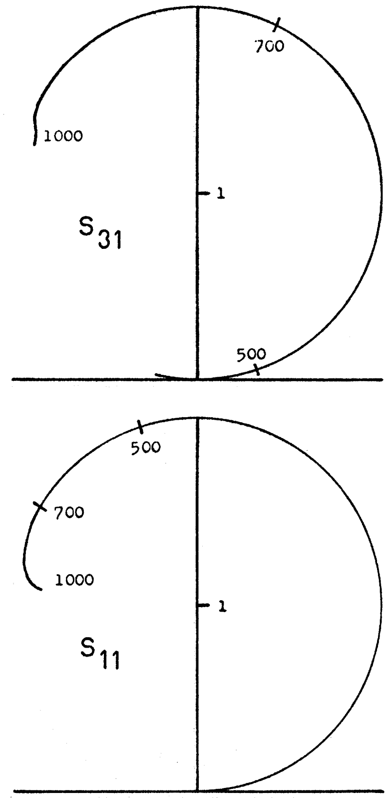

FIG. 5. Same graph as Fig. 2. Curve for both graphs predicted from solution I.

remains negative. In both our solutions, the phase shift initially becomes negative, but since $\eta \sim 1$ it swings back to the positive. Solution I exhibits a resonance at mass 1594 MeV and width 217 MeV. Rosenfeld[20] lists the S_{31} resonance as having mass 1670 MeV and width 180 MeV, so the agreement is rather good. Solution II does not display any resonance in the region plotted. However, further calculations outside of this region indicate that a resonance does occur at a mass of about 2100 MeV.

Both solutions show a resonance in the $I=\frac{1}{2}$ channel in the region plotted. Solution I yields a mass of 1417 MeV and a width of 258 MeV, while solution II gives a mass of 1355 MeV and a width of 144 MeV. This resonance is presumably to be identified with the lower of the two S_{11} resonances seen in the phase-shift analyses of either Bareyre *et al.* or Bransden *et al.* Rosenfeld lists a mass of 1570 MeV and a width of 130 MeV. The higher resonance at mass 1700 MeV does not appear in either solution.

The only inelastic process which is strongly s-wave is ηn production. Bulos *et al.*[21] observe isotropy up to an

[19] W. Bruce Richards, Charles B. Chiu, Richard D. Fondi, A. Carl Helmholz, Robert W. Kenney, Burton J. Moyer, John A. Poirier, Robert J. Cence, Vincent Z. Peterson, Navender K. Sehgal, and Victor J. Stenger, Phys. Rev. Letters **16**, 1221 (1966).

[20] Arthur H. Rosenfeld, Angela Barbaro-Galtieri, William J. Podolsky, Leroy R. Price, Paul Soding, Charles G. Wohl, Matts Roos, and William J. Willis, Rev. Mod. Phys. **39**, 1 (1967).

[21] F. Bulos, R. E. Lanou, A. E. Pifer, A. M. Shapiro, M. Widgoff, R. Panvini, A. E. Brenner, C. A. Bordner, M. E. Law, E. E. Ronat, K. Strauch, J. J. Szymanski, P. Bastien, B. B. Brabson, Y. Eisenberg, B. T. Feld, V. K. Fischer, I. A. Pless, L. Rosenson, R. K. Yamamoto, G. Calvelli, L. Guerriero, G. A. Salandin, A. Tomasin, L. Ventura, C. Voci, and F. Waldner, Phys. Rev. Letters **13**, 486 (1964).

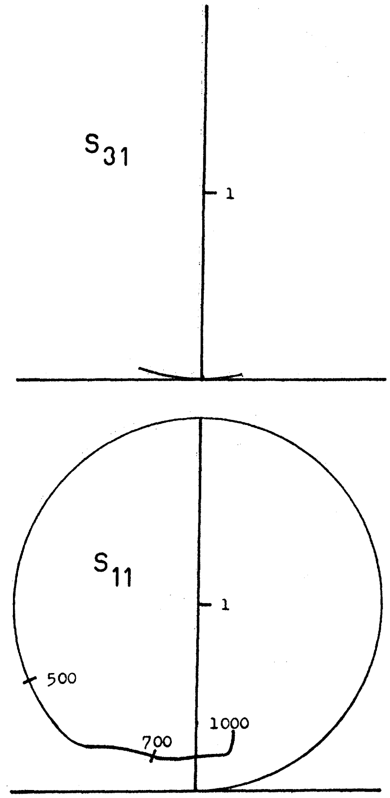

FIG. 6. Same graph as Fig. 2. Curve for both graphs predicted from solution II.

incident pion kinetic energy of approximately 950 MeV. However, Richards *et al.*,[19] using an experimental arrangement involving two additional spark chambers, have detected significant anisotropy at an energy of 655 MeV. Dobson[22] has applied the effective-range approach to the problem of ηn production and has achieved a reasonable fit to the data through 700 MeV. He is able to attribute the large ηn production cross section to an ηn virtual state which is associated with a pole in the scattering amplitude on sheet III in our diagram.

Presumably this pole is to be identified with the 1570-MeV S_{11} resonance. However, in the limit of exact $SU(6)$ symmetry, the element of the projection matrix of the **70** representation between πN and ηN is zero. So if, following Gyuk and Tuan, we place the 1570-MeV S_{11} resonance in a **70** representation, then it can contribute to ηn production only via symmetry breaking. We have plotted the experimental cross section and that predicted from solutions I and II in Fig. 7 for the process $\pi^- p \to \eta n$ where the η decays into two photons. The branching ratio R ($\eta \to 2\gamma/\eta \to$ all decays) is taken to be 0.35 in agreement with Richards. Solution I gives a ηn production cross section that is essentially zero. That for solution II does resemble the experimental cross section, but is too small by about a factor of 2.

C. *K*-Nucleon System, $Y=2$

As seen in the data of Goldhaber *et al.*,[23] the KN system appears to scatter isotropically up to an incident K-meson momentum of 600 MeV/c. In this energy range, the only two-body channel open is the elastic one, so we have but one cross section available for comparison. No resonances have been observed experimentally in this energy range.

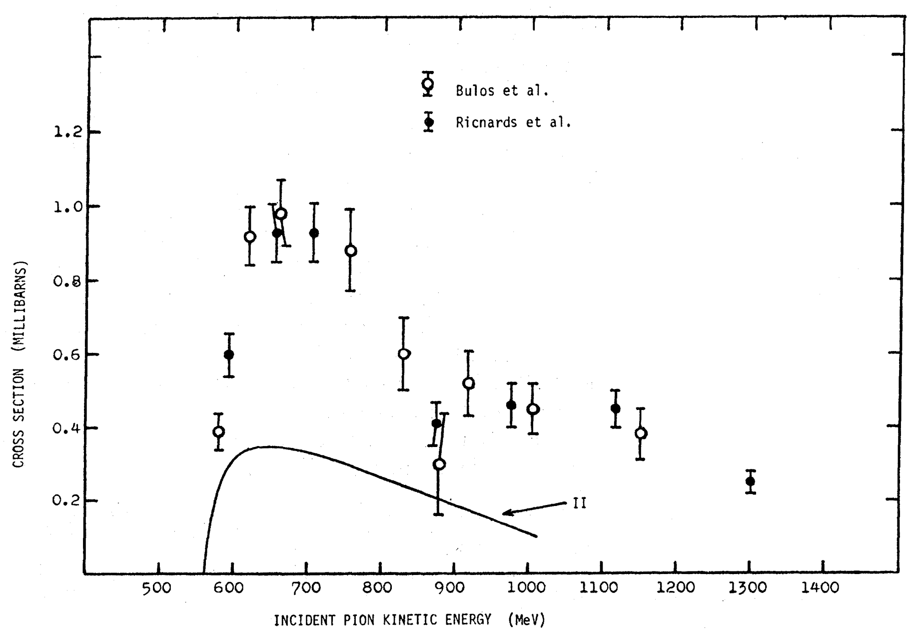

FIG. 7. Experimental and predicted cross sections for $\pi^- p \to \eta n$, $\eta \to 2\gamma$.

[22] Peter N. Dobson, Phys. Rev. **146**, 1022 (1966).
[23] S. Goldhaber, W. Chinowsky, G. Goldhaber, W. Lee, T. O'Halloran, T. Stubbs, G. M. Pjerrou, D. H. Stork, and H. K. Ticho, Phys. Rev. Letters **9**, 135 (1962).

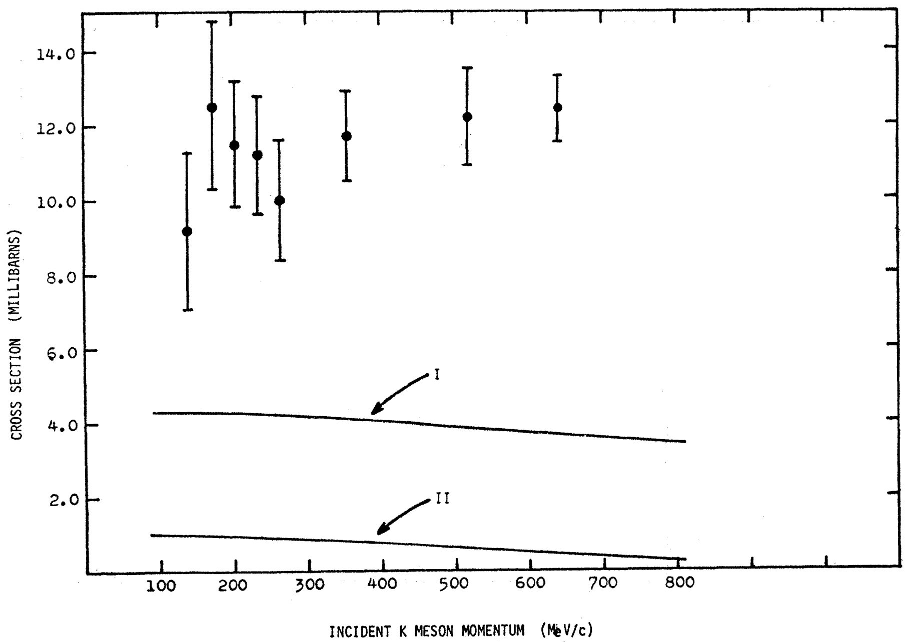

FIG. 8. Experimental and predicted cross sections for K^+p elastic scattering. Data by Goldhaber *et al.* (Ref. 23).

The K^+p elastic cross sections from both our solutions vary quite slowly over the entire energy interval, just as does the experimental cross section. However, the agreement in absolute value is not good, being off by as much as a factor of 10. Experimental and predicted cross sections are presented in Fig. 8. ReD has no zeros in either isotopic spin, and therefore no resonances are predicted.

D. $\bar{K}$-Nucleon System, $Y=0$

In the $\bar{K}N$ system, the elastic, charge-exchange, and $\Sigma\pi$ and $\Lambda\pi$ production angular distributions, as seen in the results of Sakitt *et al.*[12] and Kittel *et al.*,[13] are isotropic up to about 300-MeV/c incident K-meson momentum. The well-known theory of Dalitz and Tuan[11] is essentially a multichannel effective-range analysis which includes Coulomb effects. Hence the Dalitz-Tuan parameters reflect the behavior of the cross sections in the mentioned energy interval, and not just at threshold. Therefore, a good fit to the Dalitz-Tuan parameters with our model will mean that we can reproduce the experimental cross sections with considerable accuracy. The theory predicts a bound state of K^-p which is also a resonance in the $\Sigma\pi$ system, and may be identified with the $Y_0^*(1405)$.

In addition, the $\eta\Lambda$ production cross section from

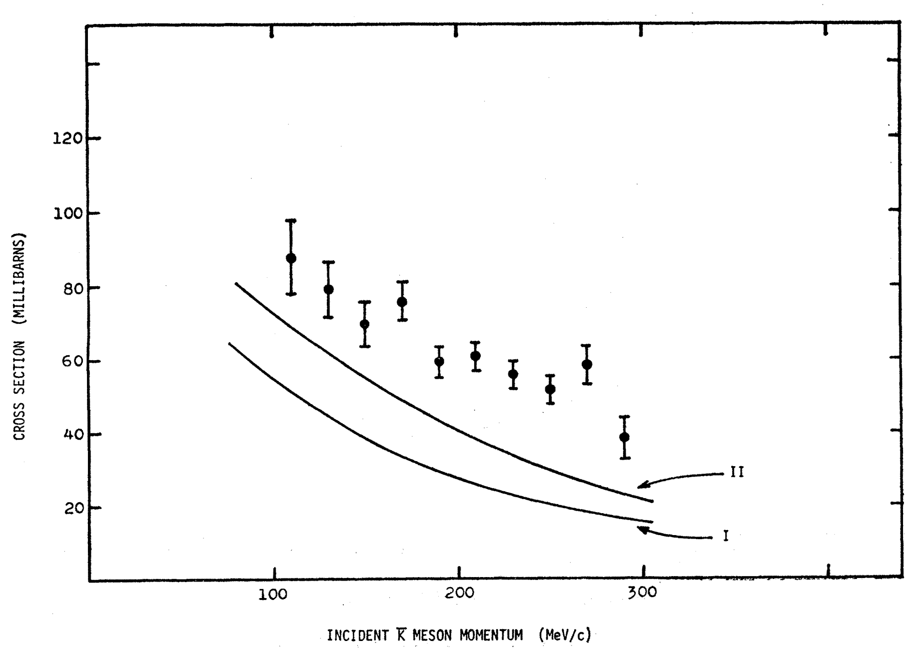

FIG. 9. Experimental and predicted cross sections for K^-p elastic scattering. Data by Sakitt *et al.* (Ref. 12).

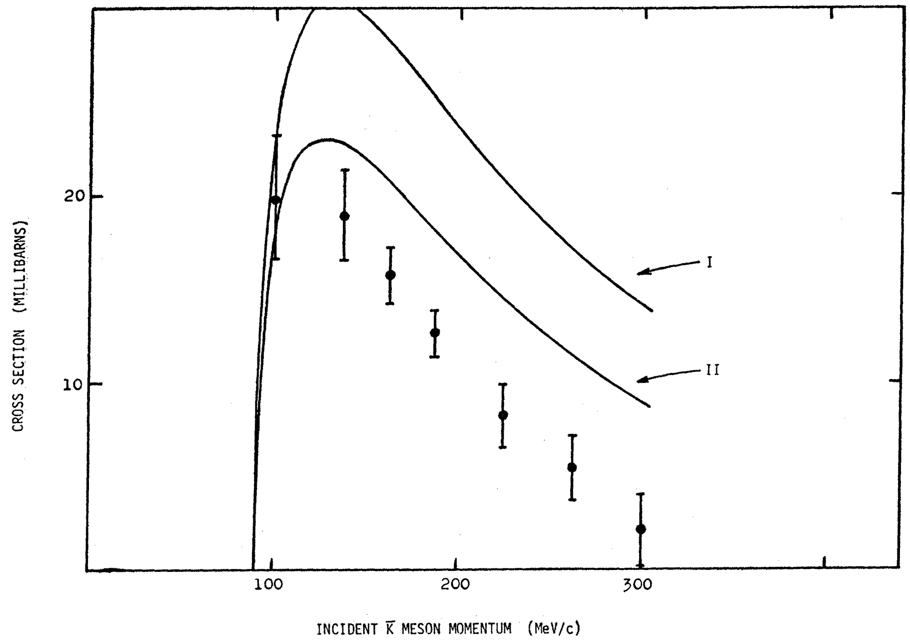

FIG. 10. Experimental and predicted cross sections for K^-p charge-exchange scattering. Data by Kittel *et al.* (Ref. 13).

threshold to a center-of-mass momentum of about 200 MeV/c is strongly s-wave. These data show a large rise and subsequent drop near threshold.[24–26] Such behavior can perhaps be explained by assuming a resonance of isotopic spin 0 and a mass of about 1670 MeV.

Predictions for the cross sections for K^-p elastic and charge-exchange scattering and $\Sigma^-\pi^+$, $\Sigma^+\pi^-$, and $\Lambda\eta$ production as calculated from our model are presented along with experimental results for comparison in Figs. 9–13. As before, the results are not too good on an absolute scale, but do show the correct qualitative behavior. In the case of elastic and charge-exchange scattering, solution II even comes close on an absolute scale. The $\Lambda\eta$ production cross section predicted by solution II is essentially zero, and therefore seems not to be shown on the graph.

Calculations of the determinant D of the inverse scattering matrix as a function of total center-of-mass

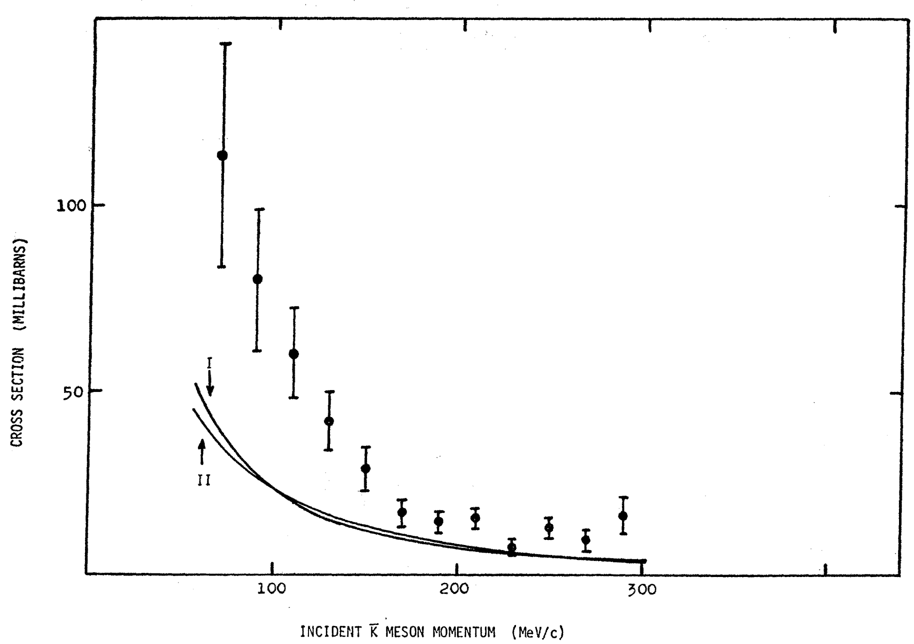

FIG. 11. Experimental and predicted cross sections for $\Sigma^-\pi^+$ production in K^-p scattering. Data by Sakitt *et al.* (Ref. 12).

[24] D. Berley, P. L. Connolly, E. L. Hart, D. C. Rahm, D. L. Stonehill, B. Thevenet, W. J. Willis, and S. S. Yamamoto, Phys. Rev. Letters **15**, 641 (1965).

[25] P. L. Bastien, J. P. Berge, O. I. Dahl, M. Ferro-Luzzi, D. H. Miller, J. J. Murray, A. H. Rosenfeld, and B. Watson, Phys. Rev. Letters **8**, 114 (1962).

[26] C. M. Rose, Jr., and D. W. Carpenter, Bull. Am. Phys. Soc. **12**, 48 (1967).

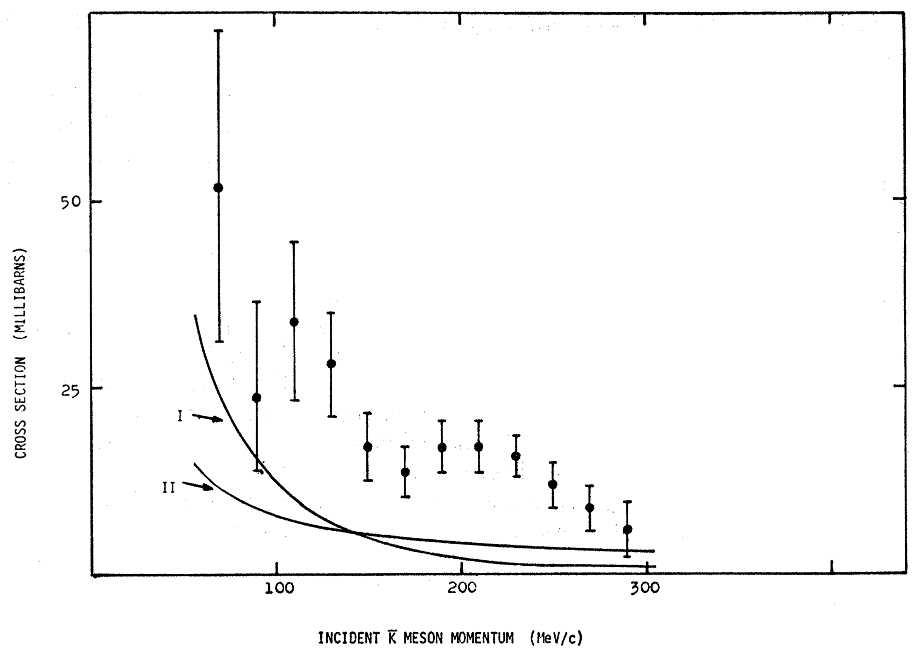

FIG. 12. Experimental and predicted cross sections for $\Sigma^+\pi^-$ production in K^-p scattering. Data by Sakitt *et al.* (Ref. 12).

energy W reveal a number of resonances. In the $I=1$ system, each solution predicts one resonance. In solution I, this resonance has a mass of 1563 MeV and a width of 105 MeV. Solution II predicts a mass of 1327 MeV, and a ridiculously small width of 0.1 MeV. Such a resonance could be placed in either an octet with the η resonances $\tilde{N}(1570)$ and $\tilde{\Lambda}(1670)$, or in a decuplet with $\tilde{N}_{3/2}{}^*(1670)$. A determination of the exact classification would involve a diagonalization of the residue of the pole according to irreducible product states.

The $I=0$ system exhibits two resonances in solution I but only one in solution II. The one resonance in common between the two solutions is clearly to be identified with the $Y_0{}^*(1405)$ which has an experimental width of 35 MeV. Solution I places this resonance at 1375 MeV with a width of 138 MeV. In solution II it has a mass of 1415 MeV and a width of 2 MeV. Both mass values are impressively close, but the widths are less accurate. The other resonance in the $I=0$ system in solution I occurs only on the $\eta\Lambda$ sheet and at 1670 MeV, very near the $\eta\Lambda$ threshold. This leads one to associate this resonance with the $\tilde{\Lambda}$ member of the η octet, which is responsible for the resonant behavior of $\Lambda\eta$ production. Our plot of the $\Lambda\eta$ production cross section does not exhibit particularly resonant behavior, but the value of the cross section is much larger than it is for solution II where

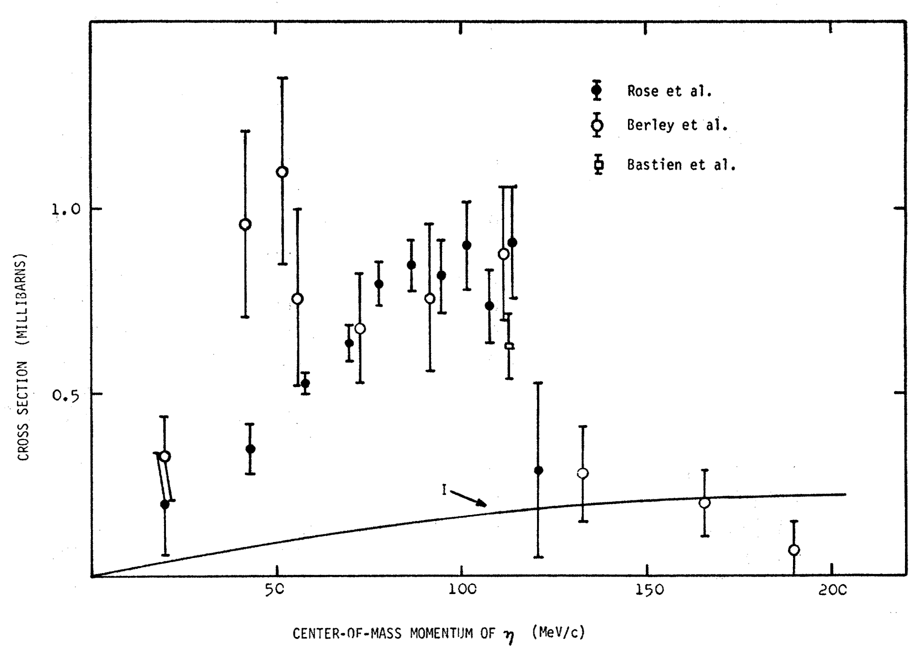

FIG. 13. Experimental and predicted cross sections for $\eta\Lambda$ production in K^-p scattering.

there is no resonance present. Although the mass is exactly right, the width is 330 MeV, compared to an experimental width of 18 MeV.

V. CONCLUSIONS

It has been seen that by including $SU(6)$ in a very simple model of meson-baryon scattering we have been able to calculate many of the s-wave resonances. Essentially all the observed resonances in the **70** representation are accounted for. Predictions of the magnitudes of the various cross sections leave something to be desired and could be improved in a number of ways. First, the $SU(6)$ symmetry breaking could be computed more exactly by taking into account the specific nature of the forces in the cross channels. Second, additional $SU(6)$ symmetry violation in the direct channel could be considered by including resonance production in higher partial waves than the s wave.

ACKNOWLEDGMENTS

The author wishes to express his gratitude to Professor Marc Ross for his valuable guidance and suggestions while this work was being performed. He would also like to thank Professor Gordon Kane for many illuminating discussions on various problems.

APPENDIX A: PROJECTION MATRICES

Matrix elements of the projection operators for the product of $SU(6)$ representations **35** and **56** onto the irreducible representations **56**, **70**, **700**, and **1134** are listed. These tables were computed from the tables of Meshkov *et al.* and those of de Swart. The states are labeled with particle names for convenience but are taken to be the eigenstates of isotopic spin I and hypercharge Y in Meshkov's paper with positive sign in all cases.

	56	70	700	1134
		$I=3/2,\ Y=1$		
$(\pi N\|\pi N)$	0	$1/16$	$1/2$	$7/16$
$(\pi N\|K\Sigma)$	0	$-1/16$	0	$1/16$
$(\pi N\|\rho N)$	0	$-1/16\sqrt{3}$	$1/2\sqrt{3}$	$-7/16\sqrt{3}$
$(\pi N\|K^*\Sigma)$	0	$1/16\sqrt{3}$	0	$-1/16\sqrt{3}$
$(\pi N\|\rho N^*)$	0	$-(\sqrt{5})/8\sqrt{3}$	$(\sqrt{5})/4\sqrt{3}$	$-(\sqrt{5})/8\sqrt{3}$
$(\pi N\|K^*Y_1^*)$	0	$-1/4\sqrt{6}$	0	$1/4\sqrt{6}$
$(\pi N\|\omega N^*)$	0	$1/8\sqrt{3}$	$1/4\sqrt{3}$	$-\sqrt{3}/8$
$(\pi N\|\phi N^*)$	0	$-1/4\sqrt{6}$	$-1/2\sqrt{6}$	$\sqrt{3}/4\sqrt{2}$
$(K\Sigma\|K\Sigma)$	0	$1/16$	$1/2$	$7/16$
$(K\Sigma\|\rho N)$	0	$1/16\sqrt{3}$	0	$-1/16\sqrt{3}$
$(K\Sigma\|K^*\Sigma)$	0	$-1/16\sqrt{3}$	$1/2\sqrt{3}$	$-7/16\sqrt{3}$
$(K\Sigma\|\rho N^*)$	0	$(\sqrt{5})/8\sqrt{3}$	0	$-(\sqrt{5})/8\sqrt{3}$
$(K\Sigma\|K^*Y_1^*)$	0	$1/4\sqrt{6}$	$-1/2\sqrt{6}$	$1/4\sqrt{6}$
$(K\Sigma\|\omega N^*)$	0	$-1/8\sqrt{3}$	$1/2\sqrt{3}$	$-\sqrt{3}/8$
$(K\Sigma\|\phi N^*)$	0	$1/4\sqrt{6}$	$1/2\sqrt{6}$	$-\sqrt{3}/4\sqrt{2}$
$(\rho N\|\rho N)$	0	$1/48$	$1/6$	$13/16$
$(\rho N\|K^*\Sigma)$	0	$-1/48$	0	$1/48$
$(\rho N\|\rho N^*)$	0	$(\sqrt{5})/24$	$(\sqrt{5})/12$	$-(\sqrt{5})/8$
$(\rho N\|K^*Y_1^*)$	0	$1/12\sqrt{2}$	0	$-1/12\sqrt{2}$
$(\rho N\|\omega N^*)$	0	$-1/24$	$1/12$	$-1/24$
$(\rho N\|\phi N^*)$	0	$1/12\sqrt{2}$	$-1/6\sqrt{2}$	$1/12\sqrt{2}$
$(K^*\Sigma\|K^*\Sigma)$	0	$1/48$	$1/6$	$13/16$
$(K^*\Sigma\|\rho N^*)$	0	$-(\sqrt{5})/24$	0	$(\sqrt{5})/24$
$(K^*\Sigma\|K^*Y_1^*)$	0	$-1/12\sqrt{2}$	$-1/6\sqrt{2}$	$1/4\sqrt{2}$
$(K^*\Sigma\|\omega N^*)$	0	$1/24$	$1/6$	$-5/24$
$(K^*\Sigma\|\phi N^*)$	0	$-1/12\sqrt{2}$	$1/6\sqrt{2}$	$-1/12\sqrt{2}$
$(\rho N^*\|\rho N^*)$	0	$5/12$	$5/24$	$3/8$
$(\rho N^*\|K^*Y_1^*)$	0	$(\sqrt{5})/6\sqrt{2}$	0	$-(\sqrt{5})/6\sqrt{2}$
$(\rho N^*\|\omega N^*)$	0	$-(\sqrt{5})/12$	$(\sqrt{5})/24$	$(\sqrt{5})/24$
$(\rho N^*\|\phi N^*)$	0	$(\sqrt{5})/6\sqrt{2}$	$-(\sqrt{5})/12\sqrt{2}$	$-(\sqrt{5})/12\sqrt{2}$
$(K^*Y_1^*\|K^*Y_1^*)$	0	$1/6$	$1/12$	$3/4$
$(K^*Y_1^*\|\omega N^*)$	0	$-1/6\sqrt{2}$	$-1/6\sqrt{2}$	$1/3\sqrt{2}$
$(K^*Y_1^*\|\phi N^*)$	0	$1/6$	$-1/12$	$-1/12$
$(\omega N^*\|\omega N^*)$	0	$1/12$	$5/24$	$17/24$
$(\omega N^*\|\phi N^*)$	0	$-1/6\sqrt{2}$	$1/12\sqrt{2}$	$1/12\sqrt{2}$
$(\phi N^*\|\phi N^*)$	0	$1/6$	$1/6$	$2/3$

	56	70	700	1134
		$I=1/2,\ Y=1$		
$(\pi N\|\pi N)$	$1/30$	$1/8$	$7/24$	$11/20$
$(\pi N\|\rho N)$	$1/6\sqrt{3}$	$1/4\sqrt{3}$	$-13/24\sqrt{3}$	$1/8\sqrt{3}$
$(\pi N\|\eta N)$	$-1/30$	0	$-1/24$	$3/40$
$(\pi N\|\omega N)$	$-1/30\sqrt{3}$	$-1/8\sqrt{3}$	$-7/24\sqrt{3}$	$3\sqrt{3}/20$
$(\pi N\|\phi N)$	$1/15\sqrt{6}$	$1/4\sqrt{6}$	$7/12\sqrt{6}$	$-3\sqrt{3}/10\sqrt{2}$
$(\pi N\|K\Sigma)$	$1/30$	$-1/16$	$-1/48$	$1/20$
$(\pi N\|K^*\Sigma)$	$-1/30\sqrt{3}$	$1/16\sqrt{3}$	$1/48\sqrt{3}$	$-1/20\sqrt{3}$
$(\pi N\|K\Lambda)$	$1/30$	$1/16$	$-1/48$	$-3/40$
$(\pi N\|K^*\Lambda)$	$1/10\sqrt{3}$	$\sqrt{3}/16$	$-1/16\sqrt{3}$	$-3\sqrt{3}/40$
$(\pi N\|\rho N^*)$	$2\sqrt{2}/15\sqrt{3}$	$-1/2\sqrt{6}$	$1/3\sqrt{6}$	$-1/10\sqrt{6}$
$(\pi N\|K^*Y_1^*)$	$\sqrt{2}/15\sqrt{3}$	$-1/4\sqrt{6}$	$-1/12\sqrt{6}$	$1/5\sqrt{6}$
$(\rho N\|\rho N)$	$5/18$	$1/6$	$31/72$	$1/8$
$(\rho N\|\eta N)$	$-1/6\sqrt{3}$	0	$-5/24\sqrt{3}$	$\sqrt{3}/8$
$(\rho N\|\omega N)$	$-1/18$	$-1/12$	$13/72$	$-1/24$
$(\rho N\|\phi N)$	$1/9\sqrt{2}$	$1/6\sqrt{2}$	$-13/36\sqrt{2}$	$1/12\sqrt{2}$
$(\rho N\|K\Sigma)$	$1/6\sqrt{3}$	$-1/8\sqrt{3}$	$-5/48\sqrt{3}$	$1/16\sqrt{3}$
$(\rho N\|K^*\Sigma)$	$-1/18$	$1/24$	$5/144$	$-1/48$
$(\rho N\|K\Lambda)$	$1/6\sqrt{3}$	$1/8\sqrt{3}$	$-5/48\sqrt{3}$	$-\sqrt{3}/16$
$(\rho N\|K^*\Lambda)$	$1/6$	$1/8$	$-5/48$	$-3/16$
$(\rho N\|\rho N^*)$	$2\sqrt{2}/9$	$-1/3\sqrt{2}$	$-1/9\sqrt{2}$	0
$(\rho N\|K^*Y_1^*)$	$\sqrt{2}/9$	$-1/6\sqrt{2}$	$-5/36\sqrt{2}$	$1/12\sqrt{2}$
$(\eta N\|\eta N)$	$1/30$	0	$7/24$	$27/40$
$(\eta N\|\omega N)$	$1/30\sqrt{3}$	0	$1/24\sqrt{3}$	$-\sqrt{3}/40$
$(\eta N\|\phi N)$	$-1/15\sqrt{6}$	0	$-1/12\sqrt{6}$	$\sqrt{3}/20\sqrt{2}$
$(\eta N\|K\Sigma)$	$-1/30$	0	$7/48$	$-9/80$
$(\eta N\|K^*\Sigma)$	$1/30\sqrt{3}$	0	$-7/48\sqrt{3}$	$3\sqrt{3}/80$
$(\eta N\|K\Lambda)$	$-1/30$	0	$7/48$	$-9/80$
$(\eta N\|K^*\Lambda)$	$-1/10\sqrt{3}$	0	$7/16\sqrt{3}$	$-9\sqrt{3}/80$
$(\eta N\|\rho N^*)$	$-2\sqrt{2}/15\sqrt{3}$	0	$-1/3\sqrt{6}$	$\sqrt{3}/5\sqrt{2}$
$(\eta N\|K^*Y_1^*)$	$-\sqrt{2}/15\sqrt{3}$	0	$7/12\sqrt{6}$	$-3\sqrt{3}/20\sqrt{2}$
$(\omega N\|\omega N)$	$1/90$	$1/24$	$19/72$	$41/60$
$(\omega N\|\phi N)$	$-1/45\sqrt{2}$	$-1/12\sqrt{2}$	$-1/36\sqrt{2}$	$\sqrt{2}/15$
$(\omega N\|K\Sigma)$	$-1/30\sqrt{3}$	$1/16\sqrt{3}$	$-5/48\sqrt{3}$	$\sqrt{3}/40$
$(\omega N\|K^*\Sigma)$	$1/90$	$-1/48$	$29/144$	$-23/120$
$(\omega N\|K\Lambda)$	$-1/30\sqrt{3}$	$-1/16\sqrt{3}$	$19/48\sqrt{3}$	$-\sqrt{3}/10$
$(\omega N\|K^*\Lambda)$	$-1/30$	$-1/16$	$-5/48$	$1/5$
$(\omega N\|\rho N^*)$	$-2\sqrt{2}/45$	$1/6\sqrt{2}$	$-1/9\sqrt{2}$	$1/30\sqrt{2}$
$(\omega N\|K^*Y_1^*)$	$-\sqrt{2}/45$	$1/12\sqrt{2}$	$7/36\sqrt{2}$	$-7/30\sqrt{2}$
$(\phi N\|\phi N)$	$1/45$	$1/12$	$5/18$	$37/60$
$(\phi N\|K\Sigma)$	$1/15\sqrt{6}$	$-1/8\sqrt{6}$	$-1/6\sqrt{6}$	$3\sqrt{3}/40\sqrt{2}$
$(\phi N\|K^*\Sigma)$	$-1/45\sqrt{2}$	$1/24\sqrt{2}$	$\sqrt{2}/9$	$-29/120\sqrt{2}$
$(\phi N\|K\Lambda)$	$1/15\sqrt{6}$	$1/8\sqrt{6}$	$1/3\sqrt{6}$	$-7\sqrt{3}/40\sqrt{2}$
$(\phi N\|K^*\Lambda)$	$1/15\sqrt{2}$	$1/8\sqrt{2}$	$-1/6\sqrt{2}$	$-1/40\sqrt{2}$
$(\phi N\|\rho N^*)$	$4/45$	$-1/6$	$1/9$	$-1/30$
$(\phi N\|K^*Y_1^*)$	$2/45$	$-1/12$	$1/18$	$-1/60$
$(K\Sigma\|K\Sigma)$	$1/30$	$1/32$	$5/48$	$133/160$
$(K\Sigma\|K^*\Sigma)$	$-1/30\sqrt{3}$	$-1/32\sqrt{3}$	$-11/48\sqrt{3}$	$47/160\sqrt{3}$
$(K\Sigma\|K\Lambda)$	$1/30$	$-1/32$	$-1/48$	$3/160$
$(K\Sigma\|K^*\Lambda)$	$1/10\sqrt{3}$	$-\sqrt{3}/32$	$5/16\sqrt{3}$	$-17\sqrt{3}/160$
$(K\Sigma\|\rho N^*)$	$2\sqrt{2}/15\sqrt{3}$	$1/4\sqrt{6}$	$-1/6\sqrt{6}$	$-7/20\sqrt{6}$
$(K\Sigma\|K^*Y_1^*)$	$\sqrt{2}/15\sqrt{3}$	$1/8\sqrt{6}$	$1/6\sqrt{6}$	$-17/40\sqrt{6}$
$(K^*\Sigma\|K^*\Sigma)$	$1/90$	$1/96$	$41/144$	$111/160$
$(K^*\Sigma\|K\Lambda)$	$-1/30\sqrt{3}$	$1/32\sqrt{3}$	$19/48\sqrt{3}$	$-21\sqrt{3}/160$
$(K^*\Sigma\|K^*\Lambda)$	$-1/30$	$1/32$	$-11/48$	$37/160$
$(K^*\Sigma\|\rho N^*)$	$-2\sqrt{2}/45$	$-1/12\sqrt{2}$	$1/18\sqrt{2}$	$7/60\sqrt{2}$
$(K^*\Sigma\|K^*Y_1^*)$	$-\sqrt{2}/45$	$-1/24\sqrt{2}$	$1/9\sqrt{2}$	$-1/40\sqrt{2}$
$(K\Lambda\|K\Lambda)$	$1/30$	$1/32$	$17/48$	$93/160$
$(K\Lambda\|K^*\Lambda)$	$1/10\sqrt{3}$	$\sqrt{3}/32$	$-1/16\sqrt{3}$	$-7\sqrt{3}/160$
$(K\Lambda\|\rho N^*)$	$2\sqrt{2}/15\sqrt{3}$	$-1/4\sqrt{6}$	$-1/6\sqrt{6}$	$\sqrt{3}/20\sqrt{2}$

	56	70	700	1134
		$I=1/2,\ Y=1$		
$(K\Lambda\|K^*Y_1^*)$	$\sqrt{2}/15\sqrt{3}$	$-1/8\sqrt{6}$	$\sqrt{2}/3\sqrt{3}$	$-9\sqrt{3}/40\sqrt{2}$
$(K^*\Lambda\|K^*\Lambda)$	1/10	3/32	5/16	79/160
$(K^*\Lambda\|\rho N^*)$	$2\sqrt{2}/15$	$-1/4\sqrt{2}$	$-1/6\sqrt{2}$	$3/20\sqrt{2}$
$(K^*\Lambda\|K^*Y_1^*)$	$\sqrt{2}/15$	$-1/8\sqrt{2}$	$1/6\sqrt{2}$	$-7/40\sqrt{2}$
$(\rho N^*\|\rho N^*)$	16/45	1/3	1/9	1/5
$(\rho N^*\|K^*Y_1^*)$	8/45	1/6	$-1/9$	$-7/30$
$(K^*Y_1^*\|K^*Y_1^*)$	4/45	1/12	5/18	11/20
		$I=1,\ Y=2$		
$(KN\|KN)$	0	0	1/2	1/2
$(KN\|K^*N)$	0	0	$1/2\sqrt{3}$	$-1/2\sqrt{3}$
$(KN\|K^*N^*)$	0	0	$1/\sqrt{6}$	$-1/\sqrt{6}$
$(K^*N\|K^*N)$	0	0	1/6	5/6
$(K^*N\|K^*N^*)$	0	0	$1/3\sqrt{2}$	$-1/3\sqrt{2}$
$(K^*N^*\|K^*N^*)$	0	0	1/3	2/3
		$I=0,\ Y=2$		
$(KN\|KN)$	0	0	1/4	3/4
$(KN\|K^*N)$	0	0	$-\sqrt{3}/4$	$\sqrt{3}/4$
$(K^*N\|K^*N)$	0	0	3/4	1/4
		$I=1,\ Y=0$		
$(\bar{K}N\|\bar{K}N)$	1/45	1/24	17/72	7/10
$(\bar{K}N\|\bar{K}^*N)$	$-1/45\sqrt{3}$	$-1/24\sqrt{3}$	$1/72\sqrt{3}$	$1/20\sqrt{3}$
$(\bar{K}N\|\pi\Sigma)$	$-2/45$	1/24	11/72	$-3/20$
$(\bar{K}N\|\rho\Sigma)$	$-4/45\sqrt{3}$	$1/12\sqrt{3}$	$-5/72\sqrt{3}$	$\sqrt{3}/40$
$(\bar{K}N\|\eta\Sigma)$	0	$-1/8\sqrt{6}$	$1/8\sqrt{6}$	0
$(\bar{K}N\|\omega\Sigma)$	$\sqrt{2}/45$	0	$-5/72\sqrt{2}$	$1/40\sqrt{2}$
$(\bar{K}N\|\phi\Sigma)$	$-1/45$	1/24	1/18	$-3/40$
$(\bar{K}N\|K\Xi)$	$-1/45$	1/48	1/72	$-1/80$
$(\bar{K}N\|K^*\Xi)$	$-1/9\sqrt{3}$	$5/48\sqrt{3}$	$5/72\sqrt{3}$	$-1/16\sqrt{3}$
$(\bar{K}N\|\rho\Lambda)$	$\sqrt{2}/45$	$-1/24\sqrt{2}$	$25/72\sqrt{2}$	$-7/20\sqrt{2}$
$(\bar{K}N\|\pi\Lambda)$	0	0	$\sqrt{3}/8\sqrt{2}$	$-\sqrt{3}/8\sqrt{2}$
$(\bar{K}N\|\bar{K}^*N^*)$	$-4\sqrt{2}/45\sqrt{3}$	$-1/3\sqrt{6}$	$1/9\sqrt{6}$	$\sqrt{2}/5\sqrt{3}$
$(\bar{K}N\|\rho Y_1^*)$	$2\sqrt{2}/45\sqrt{3}$	$-1/12\sqrt{6}$	$2\sqrt{2}/9\sqrt{3}$	$-3\sqrt{3}/20\sqrt{2}$
$(\bar{K}N\|\omega Y_1^*)$	$-2/45$	$-1/24$	1/9	$-1/40$
$(\bar{K}N\|\phi Y_1^*)$	0	$-1/12\sqrt{2}$	$-1/6\sqrt{2}$	$1/4\sqrt{2}$
$(\bar{K}N\|K^*\Xi^*)$	$2\sqrt{2}/45\sqrt{3}$	$-1/12\sqrt{6}$	$-1/18\sqrt{6}$	$1/20\sqrt{6}$
$(\bar{K}^*N\|\bar{K}^*N)$	1/135	1/72	53/216	11/15
$(\bar{K}^*N\|\pi\Sigma)$	$2/45\sqrt{3}$	$-1/24\sqrt{3}$	$-11/72\sqrt{3}$	$\sqrt{3}/20$
$(\bar{K}^*N\|\rho\Sigma)$	4/135	$-1/36$	41/216	$-23/120$
$(\bar{K}^*N\|\eta\Sigma)$	0	$1/24\sqrt{2}$	$-1/24\sqrt{2}$	0
$(\bar{K}^*N\|\omega\Sigma)$	$-\sqrt{2}/45\sqrt{3}$	0	$17/72\sqrt{6}$	$-23/120\sqrt{6}$
$(\bar{K}^*N\|\phi\Sigma)$	$1/45\sqrt{3}$	$-1/24\sqrt{3}$	$-2/9\sqrt{3}$	$29/120\sqrt{3}$
$(\bar{K}^*N\|K\Xi)$	$1/45\sqrt{3}$	$-1/48\sqrt{3}$	$-1/72\sqrt{3}$	$1/80\sqrt{3}$
$(\bar{K}^*N\|K^*\Xi)$	1/27	$-5/144$	$-5/216$	1/48
$(\bar{K}^*N\|\rho\Lambda)$	$-\sqrt{2}/45\sqrt{3}$	$1/24\sqrt{6}$	$-25/72\sqrt{6}$	$7/20\sqrt{6}$
$(\bar{K}^*N\|\pi\Lambda)$	0	0	$3/8\sqrt{2}$	$-3/8\sqrt{2}$
$(\bar{K}^*N\|\bar{K}^*N^*)$	$4\sqrt{2}/135$	$1/9\sqrt{2}$	$-1/27\sqrt{2}$	$-\sqrt{2}/15$
$(\bar{K}^*N\|\rho Y_1^*)$	$-2\sqrt{2}/135$	$1/36\sqrt{2}$	$5/27\sqrt{2}$	$-11/60\sqrt{2}$
$(\bar{K}^*N\|\omega Y_1^*)$	$2/45\sqrt{3}$	$1/24\sqrt{3}$	$1/18\sqrt{3}$	$-17/120\sqrt{3}$
$(\bar{K}^*N\|\phi Y_1^*)$	0	$1/12\sqrt{6}$	$-1/6\sqrt{6}$	$1/12\sqrt{6}$
$(\bar{K}^*N\|K^*\Xi^*)$	$-2\sqrt{2}/135$	$1/36\sqrt{2}$	$1/54\sqrt{2}$	$-1/60\sqrt{2}$
$(\pi\Sigma\|\pi\Sigma)$	4/45	1/24	7/36	27/40
$(\pi\Sigma\|\rho\Sigma)$	$8/45\sqrt{3}$	$1/12\sqrt{3}$	$-1/9\sqrt{3}$	$-\sqrt{3}/20$
$(\pi\Sigma\|\eta\Sigma)$	0	$-1/8\sqrt{6}$	$-1/4\sqrt{6}$	$\sqrt{3}/8\sqrt{2}$
$(\pi\Sigma\|\omega\Sigma)$	$-2\sqrt{2}/45$	0	$-1/9\sqrt{2}$	$1/5\sqrt{2}$
$(\pi\Sigma\|\phi\Sigma)$	2/45	1/24	5/36	$-9/40$
$(\pi\Sigma\|K\Xi)$	2/45	1/48	$-1/36$	$-3/80$

	56	70	700	1134
		$I=1,\ Y=0$		
$(\pi\Sigma\|K^*\Xi)$	$2/9\sqrt{3}$	$5/48\sqrt{3}$	$-5/36\sqrt{3}$	$-\sqrt{3}/16$
$(\pi\Sigma\|\rho\Lambda)$	$-2\sqrt{2}/45$	$-1/24\sqrt{2}$	$11/36\sqrt{2}$	$-7/40\sqrt{2}$
$(\pi\Sigma\|\pi\Lambda)$	0	0	0	0
$(\pi\Sigma\|\bar{K}^*N^*)$	$8\sqrt{2}/45\sqrt{3}$	$-1/3\sqrt{6}$	$5/18\sqrt{6}$	$-\sqrt{3}/10\sqrt{2}$
$(\pi\Sigma\|\rho Y_1^*)$	$-4\sqrt{2}/45\sqrt{3}$	$-1/12\sqrt{6}$	$1/9\sqrt{6}$	$\sqrt{3}/20\sqrt{2}$
$(\pi\Sigma\|\omega Y_1^*)$	$4/45$	$-1/24$	$1/36$	$-3/40$
$(\pi\Sigma\|\phi Y_1^*)$	0	$-1/12\sqrt{2}$	$-1/6\sqrt{2}$	$1/4\sqrt{2}$
$(\pi\Sigma\|K^*\Xi^*)$	$-4\sqrt{2}/45\sqrt{3}$	$-1/12\sqrt{6}$	$1/9\sqrt{6}$	$\sqrt{3}/20\sqrt{2}$
$(\rho\Sigma\|\rho\Sigma)$	$16/135$	$13/72$	$19/108$	$21/40$
$(\rho\Sigma\|\eta\Sigma)$	0	$-1/12\sqrt{2}$	$-1/6\sqrt{2}$	$1/4\sqrt{2}$
$(\rho\Sigma\|\omega\Sigma)$	$-4\sqrt{2}/45\sqrt{3}$	$-1/8\sqrt{6}$	$7/36\sqrt{6}$	$13/120\sqrt{6}$
$(\rho\Sigma\|\phi\Sigma)$	$4/45\sqrt{3}$	$5/24\sqrt{3}$	$-5/36\sqrt{3}$	$-19/120\sqrt{3}$
$(\rho\Sigma\|K\Xi)$	$4/45\sqrt{3}$	$11/48\sqrt{3}$	$-1/18\sqrt{3}$	$-7\sqrt{3}/80$
$(\rho\Sigma\|K^*\Xi)$	$4/27$	$19/144$	$-5/54$	$-3/16$
$(\rho\Sigma\|\rho\Lambda)$	$-4\sqrt{2}/45\sqrt{3}$	$-1/12\sqrt{6}$	$-7/18\sqrt{6}$	$13/20\sqrt{6}$
$(\rho\Sigma\|\pi\Lambda)$	0	$-1/8\sqrt{2}$	$1/4\sqrt{2}$	$-1/8\sqrt{2}$
$(\rho\Sigma\|\bar{K}^*N^*)$	$16\sqrt{2}/135$	$-\sqrt{2}/9$	$1/54\sqrt{2}$	$-1/30\sqrt{2}$
$(\rho\Sigma\|\rho Y_1^*)$	$-8\sqrt{2}/135$	$7/36\sqrt{2}$	$\sqrt{2}/27$	$-3/20\sqrt{2}$
$(\rho\Sigma\|\omega Y_1^*)$	$8/45\sqrt{3}$	$-5/24\sqrt{3}$	$-1/36\sqrt{3}$	$7/120\sqrt{3}$
$(\rho\Sigma\|\phi Y_1^*)$	0	$1/12\sqrt{6}$	$-1/6\sqrt{6}$	$1/12\sqrt{6}$
$(\rho\Sigma\|K^*\Xi^*)$	$-8\sqrt{2}/135$	$7/36\sqrt{2}$	$\sqrt{2}/27$	$-3/20\sqrt{2}$
$(\eta\Sigma\|\eta\Sigma)$	0	$1/16$	$3/8$	$9/16$
$(\eta\Sigma\|\omega\Sigma)$	0	0	0	0
$(\eta\Sigma\|\phi\Sigma)$	0	$-1/8\sqrt{6}$	$-1/4\sqrt{6}$	$\sqrt{3}/8\sqrt{2}$
$(\eta\Sigma\|K\Xi)$	0	$-1/16\sqrt{6}$	$1/4\sqrt{6}$	$-\sqrt{3}/16\sqrt{2}$
$(\eta\Sigma\|K^*\Xi)$	0	$-5/48\sqrt{2}$	$5/12\sqrt{2}$	$-5/16\sqrt{2}$
$(\eta\Sigma\|\rho\Lambda)$	0	$1/16\sqrt{3}$	$1/8\sqrt{3}$	$-\sqrt{3}/16$
$(\eta\Sigma\|\pi\Lambda)$	0	0	0	0
$(\eta\Sigma\|\bar{K}^*N^*)$	0	$1/6$	$-1/6$	0
$(\eta\Sigma\|\rho Y_1^*)$	0	$1/24$	$1/12$	$-1/8$
$(\eta\Sigma\|\omega Y_1^*)$	0	$1/8\sqrt{6}$	$1/4\sqrt{6}$	$-\sqrt{3}/4\sqrt{2}$
$(\eta\Sigma\|\phi Y_1^*)$	0	$1/8\sqrt{3}$	$1/4\sqrt{3}$	$-\sqrt{3}/8$
$(\eta\Sigma\|K^*\Xi^*)$	0	$1/24$	$-1/6$	$1/8$
$(\omega\Sigma\|\omega\Sigma)$	$2/45$	$1/48$	$25/72$	$47/80$
$(\omega\Sigma\|\phi\Sigma)$	$-\sqrt{2}/45$	$-1/24\sqrt{2}$	$7/36\sqrt{2}$	$-13/120\sqrt{2}$
$(\omega\Sigma\|K\Xi)$	$-\sqrt{2}/45$	$-1/16\sqrt{2}$	$2\sqrt{2}/9$	$-27/80\sqrt{2}$
$(\omega\Sigma\|K^*\Xi)$	$-\sqrt{2}/9\sqrt{3}$	$-1/16\sqrt{6}$	$-2\sqrt{2}/9\sqrt{3}$	$35/48\sqrt{6}$
$(\omega\Sigma\|\rho\Lambda)$	$2/45$	0	$-1/9$	$1/15$
$(\omega\Sigma\|\pi\Lambda)$	0	$1/16\sqrt{3}$	$1/8\sqrt{3}$	$-\sqrt{3}/16$
$(\omega\Sigma\|\bar{K}^*N^*)$	$-8/45\sqrt{3}$	0	$-1/18\sqrt{3}$	$7/30\sqrt{3}$
$(\omega\Sigma\|\rho Y_1^*)$	$4/45\sqrt{3}$	$-1/8\sqrt{3}$	$1/36\sqrt{3}$	$1/120\sqrt{3}$
$(\omega\Sigma\|\omega Y_1^*)$	$-2\sqrt{2}/45$	$1/24\sqrt{2}$	$5/36\sqrt{2}$	$-11/120\sqrt{2}$
$(\omega\Sigma\|\phi Y_1^*)$	0	$-1/24$	$1/12$	$-1/24$
$(\omega\Sigma\|K^*\Xi^*)$	$4/45\sqrt{3}$	$-1/8\sqrt{3}$	$-2/9\sqrt{3}$	$31/120\sqrt{3}$
$(\phi\Sigma\|\phi\Sigma)$	$1/45$	$1/12$	$5/18$	$37/60$
$(\phi\Sigma\|K\Xi)$	$1/45$	$1/12$	$7/36$	$-3/10$
$(\phi\Sigma\|K^*\Xi)$	$1/9\sqrt{3}$	$1/6\sqrt{3}$	$-13/36\sqrt{3}$	$1/12\sqrt{3}$
$(\phi\Sigma\|\rho\Lambda)$	$-\sqrt{2}/45$	$-1/24\sqrt{2}$	$7/36\sqrt{2}$	$-13/120\sqrt{2}$
$(\phi\Sigma\|\pi\Lambda)$	0	$-1/8\sqrt{6}$	$-1/4\sqrt{6}$	$\sqrt{3}/8\sqrt{2}$
$(\phi\Sigma\|\bar{K}^*N^*)$	$4\sqrt{2}/45\sqrt{3}$	$-1/3\sqrt{6}$	$\sqrt{2}/9\sqrt{3}$	$-1/15\sqrt{6}$
$(\phi\Sigma\|\rho Y_1^*)$	$-2\sqrt{2}/45\sqrt{3}$	$1/6\sqrt{6}$	$-1/9\sqrt{6}$	$1/30\sqrt{6}$
$(\phi\Sigma\|\omega Y_1^*)$	$2/45$	$-1/12$	$1/18$	$-1/60$
$(\phi\Sigma\|\phi Y_1^*)$	0	0	0	0
$(\phi\Sigma\|K^*\Xi^*)$	$-2\sqrt{2}/45\sqrt{3}$	$1/6\sqrt{6}$	$-1/9\sqrt{6}$	$1/30\sqrt{6}$
$(K\Xi\|K\Xi)$	$1/45$	$5/48$	$13/36$	$41/80$
$(K\Xi\|K^*\Xi)$	$1/9\sqrt{3}$	$7/48\sqrt{3}$	$-7/36\sqrt{3}$	$-1/16\sqrt{3}$
$(K\Xi\|\rho\Lambda)$	$-\sqrt{2}/45$	$-1/48\sqrt{2}$	$1/36\sqrt{2}$	$3/80\sqrt{2}$
$(K\Xi\|\pi\Lambda)$	0	$-\sqrt{3}/16\sqrt{2}$	0	$\sqrt{3}/16\sqrt{2}$
$(K\Xi\|\bar{K}^*N^*)$	$4\sqrt{2}/45\sqrt{3}$	$-1/6\sqrt{6}$	$-1/9\sqrt{6}$	$1/10\sqrt{6}$

	56	70	700	1134
		$I=1,\ Y=0$		
$(K\Xi\|\rho Y_1^*)$	$-2\sqrt{2}/45\sqrt{3}$	$1/3\sqrt{6}$	$1/18\sqrt{6}$	$-\sqrt{3}/10\sqrt{2}$
$(K\Xi\|\omega Y_1^*)$	$2/45$	$-1/12$	$5/36$	$-1/10$
$(K\Xi\|\phi Y_1^*)$	0	$1/12\sqrt{2}$	$1/6\sqrt{2}$	$-1/4\sqrt{2}$
$(K\Xi\|K^*\Xi^*)$	$-2\sqrt{2}/45\sqrt{3}$	$1/3\sqrt{6}$	$-2\sqrt{2}/9\sqrt{3}$	$1/5\sqrt{6}$
$(K^*\Xi\|K^*\Xi)$	$5/27$	$17/144$	$37/108$	$17/48$
$(K^*\Xi\|\rho\Lambda)$	$-\sqrt{2}/9\sqrt{3}$	$-5/48\sqrt{6}$	$5/36\sqrt{6}$	$\sqrt{3}/16\sqrt{2}$
$(K^*\Xi\|\pi\Lambda)$	0	$-1/16\sqrt{2}$	0	$1/16\sqrt{2}$
$(K^*\Xi\|\bar{K}^*N^*)$	$4\sqrt{2}/27$	$-5/18\sqrt{2}$	$-5/27\sqrt{2}$	$1/6\sqrt{2}$
$(K^*\Xi\|\rho Y_1^*)$	$-2\sqrt{2}/27$	$1/18\sqrt{2}$	$5/54\sqrt{2}$	0
$(K^*\Xi\|\omega Y_1^*)$	$2/9\sqrt{3}$	$-1/6\sqrt{3}$	$1/36\sqrt{3}$	$-1/12\sqrt{3}$
$(K^*\Xi\|\phi Y_1^*)$	0	$-1/12\sqrt{6}$	$1/6\sqrt{6}$	$-1/12\sqrt{6}$
$(K^*\Xi\|K^*\Xi^*)$	$-2\sqrt{2}/27$	$1/18\sqrt{2}$	$-\sqrt{2}/27$	$1/6\sqrt{2}$
$(\rho\Lambda\|\rho\Lambda)$	$2/45$	$1/48$	$25/72$	$27/80$
$(\rho\Lambda\|\pi\Lambda)$	0	0	0	0
$(\rho\Lambda\|\bar{K}^*N^*)$	$-8/45\sqrt{3}$	$1/6\sqrt{3}$	$1/9\sqrt{3}$	$-1/10\sqrt{3}$
$(\rho\Lambda\|\rho Y_1^*)$	$4/45\sqrt{3}$	$1/24\sqrt{3}$	$7/36\sqrt{3}$	$-13/40\sqrt{3}$
$(\rho\Lambda\|\omega Y_1^*)$	$-2\sqrt{2}/45$	$1/24\sqrt{2}$	$5/36\sqrt{2}$	$-11/120\sqrt{2}$
$(\rho\Lambda\|\phi Y_1^*)$	0	$1/24$	$-1/12$	$1/24$
$(\rho\Lambda\|K^*\Xi^*)$	$4/45\sqrt{3}$	$1/24\sqrt{3}$	$-1/18\sqrt{3}$	$-\sqrt{3}/40$
$(\pi\Lambda\|\pi\Lambda)$	0	$1/16$	$3/8$	$9/16$
$(\pi\Lambda\|\bar{K}^*N^*)$	0	0	0	0
$(\pi\Lambda\|\rho Y_1^*)$	0	$-1/8$	$1/4$	$-1/8$
$(\pi\Lambda\|\omega Y_1^*)$	0	$1/8\sqrt{6}$	$1/4\sqrt{6}$	$-\sqrt{3}/8\sqrt{2}$
$(\pi\Lambda\|\phi Y_1^*)$	0	$-1/8\sqrt{3}$	$-1/4\sqrt{3}$	$\sqrt{3}/8$
$(\pi\Lambda\|K^*\Xi^*)$	0	$-1/8$	0	$1/8$
$(\bar{K}^*N^*\|\bar{K}^*N^*)$	$32/135$	$4/9$	$11/108$	$13/60$
$(\bar{K}^*N^*\|\rho Y_1^*)$	$-16/135$	$1/9$	$-1/108$	$1/60$
$(\bar{K}^*N^*\|\omega Y_1^*)$	$8\sqrt{2}/45\sqrt{3}$	$1/3\sqrt{6}$	$-1/18\sqrt{6}$	$-19/30\sqrt{6}$
$(\bar{K}^*N^*\|\phi Y_1^*)$	0	$1/3\sqrt{3}$	$-1/6\sqrt{3}$	$-1/6\sqrt{3}$
$(\bar{K}^*N^*\|K^*\Xi^*)$	$-16/135$	$1/9$	$2/27$	$-1/15$
$(\rho Y_1^*\|\rho Y_1^*)$	$8/135$	$5/18$	$23/108$	$9/20$
$(\rho Y_1^*\|\omega Y_1^*)$	$-4\sqrt{2}/45\sqrt{3}$	$-1/6\sqrt{6}$	$5/18\sqrt{6}$	$1/15\sqrt{6}$
$(\rho Y_1^*\|\phi Y_1^*)$	0	$1/3\sqrt{3}$	$-1/6\sqrt{3}$	$-1/6\sqrt{3}$
$(\rho Y_1^*\|K^*\Xi^*)$	$8/135$	$5/18$	$-1/27$	$-3/10$
$(\omega Y_1^*\|\omega Y_1^*)$	$4/45$	$1/12$	$1/9$	$43/60$
$(\omega Y_1^*\|\phi Y_1^*)$	0	0	0	0
$(\omega Y_1^*\|K^*\Xi^*)$	$-4\sqrt{2}/45\sqrt{3}$	$-1/6\sqrt{6}$	$-\sqrt{2}/9\sqrt{3}$	$17/30\sqrt{6}$
$(\phi Y_1^*\|\phi Y_1^*)$	0	$1/6$	$1/6$	$2/3$
$(\phi Y_1^*\|K^*\Xi^*)$	0	$1/3\sqrt{3}$	$-1/6\sqrt{3}$	$-1/6\sqrt{3}$
$(K^*\Xi^*\|K^*\Xi^*)$	$8/135$	$5/18$	$7/54$	$8/15$
		$I=0,\ Y=0$		
$(\bar{K}N\|\bar{K}N)$	$1/15$	$1/8$	$5/24$	$3/5$
$(\bar{K}N\|\bar{K}^*N)$	$1/5\sqrt{3}$	$\sqrt{3}/8$	$-1/8\sqrt{3}$	$-3\sqrt{3}/20$
$(\bar{K}N\|\pi\Sigma)$	0	0	$\sqrt{3}/8\sqrt{2}$	$-\sqrt{3}/8\sqrt{2}$
$(\bar{K}N\|\rho\Sigma)$	$\sqrt{2}/15$	$-1/8\sqrt{2}$	$-5/24\sqrt{2}$	$1/5\sqrt{2}$
$(\bar{K}N\|K\Xi)$	$1/15$	$-1/16$	$-1/24$	$3/80$
$(\bar{K}N\|K^*\Xi)$	$1/15\sqrt{3}$	$-1/16\sqrt{3}$	$-1/24\sqrt{3}$	$\sqrt{3}/80$
$(\bar{K}N\|\eta\Lambda)$	0	$1/8\sqrt{2}$	$-1/8\sqrt{2}$	0
$(\bar{K}N\|\omega\Lambda)$	$\sqrt{2}/15\sqrt{3}$	$1/4\sqrt{6}$	$-11/24\sqrt{6}$	$\sqrt{3}/40\sqrt{2}$
$(\bar{K}N\|\phi\Lambda)$	$1/15\sqrt{3}$	$1/8\sqrt{3}$	$1/3\sqrt{3}$	$-7\sqrt{3}/40$
$(\bar{K}N\|\rho Y_1^*)$	$2/15$	$-1/8$	$1/6$	$-7/40$
$(\bar{K}N\|K^*\Xi^*)$	$2\sqrt{2}/15\sqrt{3}$	$-1/4\sqrt{6}$	$-1/6\sqrt{6}$	$\sqrt{3}/20\sqrt{2}$
$(\bar{K}^*N\|\bar{K}^*N)$	$1/5$	$3/8$	$1/8$	$3/10$
$(\bar{K}^*N\|\pi\Sigma)$	0	0	$-1/8\sqrt{2}$	$1/8\sqrt{2}$
$(\bar{K}^*N\|\rho\Sigma)$	$\sqrt{2}/5\sqrt{3}$	$-\sqrt{3}/8\sqrt{2}$	$\sqrt{3}/8\sqrt{2}$	$-\sqrt{2}/5\sqrt{3}$
$(\bar{K}^*N\|K\Xi)$	$1/5\sqrt{3}$	$-\sqrt{3}/16$	$-1/8\sqrt{3}$	$3\sqrt{3}/80$
$(\bar{K}^*N\|K^*\Xi)$	$1/15$	$-1/16$	$-1/24$	$3/80$
$(\bar{K}^*N\|\eta\Lambda)$	0	$\sqrt{3}/8\sqrt{2}$	$-\sqrt{3}/8\sqrt{2}$	0

	56	70	700	1134
		$I=0,\ Y=0$		
$(\bar{K}^*N\|\omega\Lambda)$	$\sqrt{2}/15$	$1/4\sqrt{2}$	$1/24\sqrt{2}$	$-17/40\sqrt{2}$
$(\bar{K}^*N\|\phi\Lambda)$	$1/15$	$1/8$	$-1/6$	$-1/40$
$(\bar{K}^*N\|\rho Y_1^*)$	$2/5\sqrt{3}$	$-\sqrt{3}/8$	0	$-1/40\sqrt{3}$
$(\bar{K}^*N\|K^*\Xi^*)$	$2\sqrt{2}/15$	$-1/4\sqrt{2}$	$-1/6\sqrt{2}$	$3/20\sqrt{2}$
$(\pi\Sigma\|\pi\Sigma)$	0	$3/16$	$1/8$	$11/16$
$(\pi\Sigma\|\rho\Sigma)$	0	$\sqrt{3}/8$	$-1/4\sqrt{3}$	$-1/8\sqrt{3}$
$(\pi\Sigma\|K\Xi)$	0	$\sqrt{3}/16\sqrt{2}$	0	$-\sqrt{3}/16\sqrt{2}$
$(\pi\Sigma\|K^*\Xi)$	0	$5/16\sqrt{2}$	0	$-5/16\sqrt{2}$
$(\pi\Sigma\|\eta\Lambda)$	0	0	0	0
$(\pi\Sigma\|\omega\Lambda)$	0	$-1/16$	$-1/8$	$3/16$
$(\pi\Sigma\|\phi\Lambda)$	0	$1/8\sqrt{2}$	$1/4\sqrt{2}$	$-3/8\sqrt{2}$
$(\pi\Sigma\|\rho Y_1^*)$	0	$-\sqrt{3}/8\sqrt{2}$	$1/4\sqrt{6}$	$1/8\sqrt{6}$
$(\pi\Sigma\|K^*\Xi^*)$	0	$-1/8$	0	$1/8$
$(\rho\Sigma\|\rho\Sigma)$	$2/15$	$5/16$	$5/24$	$83/240$
$(\rho\Sigma\|K\Xi)$	$\sqrt{2}/15$	$3/16\sqrt{2}$	$-1/12\sqrt{2}$	$-19/80\sqrt{2}$
$(\rho\Sigma\|K^*\Xi)$	$\sqrt{2}/15\sqrt{3}$	$11/16\sqrt{6}$	$-1/12\sqrt{6}$	$-59/80\sqrt{6}$
$(\rho\Sigma\|\eta\Lambda)$	0	$-1/16$	$-1/8$	$3/16$
$(\rho\Sigma\|\omega\Lambda)$	$2/15\sqrt{3}$	$-1/4\sqrt{3}$	$1/6\sqrt{3}$	$-1/20\sqrt{3}$
$(\rho\Sigma\|\phi\Lambda)$	$\sqrt{2}/15\sqrt{3}$	$1/8\sqrt{6}$	$-7/12\sqrt{6}$	$13/40\sqrt{6}$
$(\rho\Sigma\|\rho Y_1^*)$	$2\sqrt{2}/15$	$-1/8\sqrt{2}$	$-1/12\sqrt{2}$	$-7/120\sqrt{2}$
$(\rho\Sigma\|K^*\Xi^*)$	$4/15\sqrt{3}$	$-1/8\sqrt{3}$	$-1/6\sqrt{3}$	$1/40\sqrt{3}$
$(K\Xi\|K\Xi)$	$1/15$	$1/16$	$1/12$	$63/80$
$(K\Xi\|K^*\Xi)$	$1/15\sqrt{3}$	$\sqrt{3}/16$	$1/12\sqrt{3}$	$-9\sqrt{3}/80$
$(K\Xi\|\eta\Lambda)$	0	$-1/16\sqrt{2}$	$1/4\sqrt{2}$	$-3/16\sqrt{2}$
$(K\Xi\|\omega\Lambda)$	$\sqrt{2}/15\sqrt{3}$	$-\sqrt{3}/16\sqrt{2}$	$1/6\sqrt{6}$	$-3\sqrt{3}/80\sqrt{2}$
$(K\Xi\|\phi\Lambda)$	$1/15\sqrt{3}$	0	$1/12\sqrt{3}$	$-\sqrt{3}/20$
$(K\Xi\|\rho Y_1^*)$	$2/15$	0	$-1/12$	$-1/20$
$(K\Xi\|K^*\Xi^*)$	$2\sqrt{2}/15\sqrt{3}$	0	$1/3\sqrt{6}$	$-\sqrt{3}/5\sqrt{2}$
$(K^*\Xi\|K^*\Xi)$	$1/45$	$13/48$	$1/36$	$163/240$
$(K^*\Xi\|\eta\Lambda)$	0	$-1/16\sqrt{6}$	$1/4\sqrt{6}$	$-\sqrt{3}/16\sqrt{2}$
$(K^*\Xi\|\omega\Lambda)$	$\sqrt{2}/45$	$-7/48\sqrt{2}$	$1/18\sqrt{2}$	$11/240\sqrt{2}$
$(K^*\Xi\|\phi\Lambda)$	$1/45$	$1/12$	$1/36$	$-2/15$
$(K^*\Xi\|\rho Y_1^*)$	$2/15\sqrt{3}$	$-1/4\sqrt{3}$	$-1/12\sqrt{3}$	$1/5\sqrt{3}$
$(K^*\Xi\|K^*\Xi^*)$	$2\sqrt{2}/45$	$-1/6\sqrt{2}$	$1/9\sqrt{2}$	$-1/30\sqrt{2}$
$(\eta\Lambda\|\eta\Lambda)$	0	$1/16$	$3/8$	$9/16$
$(\eta\Lambda\|\omega\Lambda)$	0	$1/8\sqrt{3}$	$1/4\sqrt{3}$	$-\sqrt{3}/8$
$(\eta\Lambda\|\phi\Lambda)$	0	$1/8\sqrt{6}$	$1/4\sqrt{6}$	$-\sqrt{3}/8\sqrt{2}$
$(\eta\Lambda\|\rho Y_1^*)$	0	$-1/8\sqrt{2}$	$-1/4\sqrt{2}$	$3/8\sqrt{2}$
$(\eta\Lambda\|K^*\Xi^*)$	0	$-1/8\sqrt{3}$	$1/2\sqrt{3}$	$-\sqrt{3}/8$
$(\omega\Lambda\|\omega\Lambda)$	$2/45$	$5/48$	$13/72$	$161/240$
$(\omega\Lambda\|\phi\Lambda)$	$\sqrt{2}/45$	$1/24\sqrt{2}$	$-7/36\sqrt{2}$	$13/120\sqrt{2}$
$(\omega\Lambda\|\rho Y_1^*)$	$2\sqrt{2}/15\sqrt{3}$	$-1/8\sqrt{6}$	$-5/12\sqrt{6}$	$11/40\sqrt{6}$
$(\omega\Lambda\|K^*\Xi^*)$	$4/45$	$-1/24$	$1/9$	$-19/120$
$(\phi\Lambda\|\phi\Lambda)$	$1/45$	$1/12$	$5/18$	$37/60$
$(\phi\Lambda\|\rho Y_1^*)$	$2/15\sqrt{3}$	$-1/4\sqrt{3}$	$1/6\sqrt{3}$	$-1/20\sqrt{3}$
$(\phi\Lambda\|K^*\Xi^*)$	$2\sqrt{2}/45$	$-1/6\sqrt{2}$	$1/9\sqrt{2}$	$-1/30\sqrt{2}$
$(\rho Y_1^*\|\rho Y_1^*)$	$4/15$	$1/4$	$1/6$	$19/60$
$(\rho Y_1^*\|K^*\Xi^*)$	$4\sqrt{2}/15\sqrt{3}$	$1/2\sqrt{6}$	$-1/3\sqrt{6}$	$-7/10\sqrt{6}$
$(K^*\Xi^*\|K^*\Xi^*)$	$8/45$	$1/6$	$2/9$	$13/30$